SEISMOFLOW - DATA AUGMENTATION FOR THE CLASS IMBALANCE PROBLEM

Ruy Luiz Milidiú
Department of Computer Science
Pontifical Catholic University of Rio de Janeiro
Rio de Janeiro, Brazil
milidiu@inf.puc-rio.br

Luis Felipe Müller
Department of Computer Science
Pontifical Catholic University of Rio de Janeiro
Rio de Janeiro, Brazil
lhenriques@inf.puc-rio.br

September 3, 2020

ABSTRACT

In several application areas, such as medical diagnosis, spam filtering, fraud detection, and seismic data analysis, it is very usual to find relevant classification tasks where some class occurrences are rare. This is the so called class imbalance problem, which is a challenge in machine learning. In this work, we propose the *SeismoFlow* a flow-based generative model to create synthetic samples, aiming to address the class imbalance. Inspired by the Glow model, it uses interpolation on the learned latent space to produce synthetic samples for one rare class. We apply our approach to the development of a seismogram signal quality classifier. We introduce a dataset composed of 5.223 seismograms that are distributed between the *good*, *medium*, and *bad* classes and with their respective frequencies of 66.68%, 31.54%, and 1.76%. Our methodology is evaluated on a stratified 10-fold cross-validation setting, using the *Miniception* model as a baseline, and assessing the effects of adding the generated samples on the training set of each iteration. In our experiments, we achieve an improvement of 13.9% on the rare class F_1 score, while not hurting the metric value for the other classes and thus observing on the overall accuracy improvement. Our empirical findings indicate that our method can generate high-quality synthetic seismograms with realistic looking and sufficient plurality to help the *Miniception* model to overcome the class imbalance problem. We believe that our results are a step forward in solving both the task of seismogram signal quality classification and class imbalance.

Keywords Class Imbalance · Neural Networks · Machine Learning · Normalizing Flows · Invertible Neural Networks

1 Introduction

The class imbalance problem is a challenge in machine learning classification tasks [1]. The problem occurs when there is a rare and very low-frequency class in the training set, making many machine learning algorithms, such as neural networks, struggle to learn to classify the low-frequency class [2]. Such a scenario appears in many different areas, such as medical diagnosis, spam filtering, fraud detection, and seismic data analysis.

In this work, we propose the *SeismoFlow* a flow-based generative model to create synthetic samples, aiming to address the class imbalance. Inspired by the Glow model [3], it uses interpolation on the learned latent space to produce synthetic samples for the rare class. We apply our approach to the development of a seismogram signal quality classifier.

In geophysics, seismograms are used for a variety of tasks, such as to estimate subsurface structural settings, stratigraphic geometry features, and potential hydrocarbon deposit locations [4]. Therefore, one of the most important and time-consuming tasks to perform these analyses is the creation of a robust and credible dataset [5].

Currently, a huge amount of seismic data is routinely available, but the quality of this data varies enormously. For example, data from a seismic reflection surveying is usually corrupted by background noise, instrument malfunction, or errors introduced during data storage and retrieval [5]. This corrupted data may, therefore, lead to unusable seismograms.

Moreover, for many applications, the poor-quality data will distort results significantly, which makes it impossible to use all available data blindly. Thus, classifying the data according to its quality is mandatory when dealing with seismic data.

We introduce a dataset composed of 5.223 seismograms that are distributed between the *good*, *medium*, and *bad* classes and with their respective frequencies of 66.68%, 31.54%, and 1.76%.

We evaluate our methodology on a stratified 10-fold cross-validation setting [6], using the *Miniception* model [] as a baseline and assessing the effects of adding the generated samples on the training set of each iteration. In our experiments, we achieve an improvement of 13.9% on the low-frequency class F_1 score, while not hurting the metric value for the other classes and thus observing an overall accuracy improvement. Our empirical findings indicate that our method can generate high-quality synthetic samples with realistic looking and sufficient plurality to help a classifier to overcome the class imbalance problem. We believe that our results are a step forward in solving both the task of seismogram signal quality classification and class imbalance.

The remaining of this paper is organized as follows. In Section 2, we perform a brief review of the related works on generative normalizing flow models. In section 3 we give a brief introduction to normalizing flow models and its loss formulation. Section 4 describes the proposed *SeismoFlow* model, its layers and the normalization schemes added to the loss. Section 5 describes our experiments, the setups, and reports our findings. Finally, section 6 concludes with a short discussion section.

2 Related Work

Currently, learning widely applicable generative models is an active area of research. Many advances have been achieved, mostly with likelihood-based methods [7, 8, 9, 10, 11, 3] and generative adversarial networks (GANs) [12].

Likelihood-based models such as autoregressive models [13, 8, 14, 15], Variational autoencoders (VAEs) [7] and Flow-based generative models [9, 11, 3], learn from the optimization of a lower bound on the log-likelihood of the data. In contrast, GANs [12] learn in an adversarial training setting. In such a procedure, the generator network creates new data instances, while the discriminator network evaluates the samples for authenticity. GANs are known for their ability to synthesize large and realistic images [16]. On the other hand, the general lack of full support over the data points [17], the absence of encoders to the latent-space, the optimization instability, and the difficulty of evaluating overfitting and generalization, are some of the well-known disadvantages of GANs.

In likelihood-based models, the variational autoencoder (VAE) algorithm [7, 18] simultaneously learns a generative network and a matched approximate inference network. The generative network maps the Gaussian latent variables to samples. In its turn, by exploiting the reparametrization trick [19], the approximate inference network maps samples to a semantically meaningful latent representation. The approximation in the inference process limits the model's ability to learn high dimensional deep representations. This limitation motivates a variety of works to attempt to improve the approximate inferences in variational autoencoders [20, 21, 22, 23, 24, 25].

Autoregressive models typically avoid such approximations by abstaining from using latent variables, while usually retaining a great deal of flexibility [26, 27, 28]. This class of algorithms simplifies the log-likelihood evaluation and sampling using the probability chain rule to decompose the joint distribution into a product of conditionals according to a fixed ordering over dimensions. Usually, works in this line of research use long-short term memory [13] recurrent networks, and residual networks [29, 30] to learn generative image and language models [31, 10, 32]. The ordering of the dimensions, although often arbitrary, can be critical to the training of the model [33]. Furthermore, synthesis is difficult to parallelize, and its computational effort is proportional to the data dimensionality [13, 8, 10, 14, 15, 34]. Additionally, there is no natural latent representation associated with autoregressive models.

Finally, normalizing flow models [9, 11, 3], allow exact latent-variable inference and log-likelihood evaluation without approximation. The approximation absence leads to accurate inference, and it also enables data direct log-likelihood optimization, instead of a lower bound of it [3]. For this reason, using such models, data points can be directly represented in a latent space, making it easy to sample from the model, perform semantic manipulations of the latent variables, interpolate data points, and evaluate the likelihood of a sample. Flow based models are usually built by stacking individual and simple invertible transformations that map the observed data to a standard Gaussian latent variable [9, 11, 3, 21, 25, 35, 36]. The number of stacked layers needed to map the observations to Gaussian space could be a limiting constraint to the model, due to the extra memory needed to compute the gradients during training. But, as the RevNet paper [37] showed that computing gradients in reversible neural networks requires a constant amount of memory, instead of linear in their depth, it does not become a problem in practice.

This work builds upon the ideas and flows proposed in Nice [9], RealNVP [11], and Glow [3] to create synthetic augmentations of a low frequency class in an imbalanced dataset.

3 Flow based Models

Let $x \in \mathbb{R}^M$ be a random vector with the true distribution $p(x)$. Given an i.i.d. dataset $\mathcal{D}$ and the discrete data $x \sim p(x)$, the log-likelihood objective is equivalent to minimizing:

$$\mathcal{L}(\mathcal{D}) = \frac{1}{N} \sum_{i=1}^{N} -log \ p(x^{(i)}) \tag{1}$$

In the case of continuous data x, we first define

$$\tilde{x}^{(i)} = x^{(i)} + u$$

with $u \sim U(0, a)$, where a is the data discretization level. Then, we minimize

$$\mathcal{L}(\mathcal{D}) \simeq \frac{1}{N} \sum_{i=1}^{N} -log \ p(\tilde{x}^{(i)}) + c \tag{2}$$

where $c = -M \cdot log \ a$ and M is the x dimensionality. The loss defined in equations 1 and 2 measures the expected compression cost in bits or nats [11].

The flow model

$$z = f_\theta(x), \tag{3}$$

where θ is the model's parameter collection, is constructed by composing a sequence of L invertible flows

$$z = f_\theta(x) = f^{(1)}(\ldots(f^{(L)}(x)), \tag{4}$$

the so called normalizing flow [21]. Each $f^{(i)}$ component has a tractable inverse and a tractable Jacobian determinant. Therefore, the generative process is defined as:

$$z \sim p_z(f_\theta(x)) \tag{5}$$

$$x = f_\theta^{-1}(z) \tag{6}$$

where p_z is typically a predefined simple and tractable distribution, for example, a standard Gaussian distribution. Thus, the function f_θ is bijective, such that given a data point x latent-variable inference is made by $z = f_\theta(x)$.

The function f_θ is learned via maximum likelihood through the change of variable formula:

$$p(x) = p_z(f_\theta(x)) \left| det \left(\frac{\partial f_\theta(x)}{\partial x} \right) \right| \tag{7}$$

Since f_θ is a composition of functions, the log probability density function given z, under equation 7, is written as:

$$log \ p(x) = log \ p_z(f_\theta(x)) + log \left| det \left(\frac{\partial z}{\partial x} \right) \right|$$
$$= log \ p_z(f_\theta(x)) + \sum_{i=1}^{K} log \left| det \left(\frac{\partial h^{(i)}}{\partial h^{(i-1)}} \right) \right| \tag{8}$$

where $h^{(0)} = x$ is the observed data, $h^{(i)}$ is the ith hidden layer output, and $h^{(K)} = f_\theta(x) = z$ is the encoded latent variable. Also, $\left| det(\partial h^{(i)}/\partial h^{(i-1)}) \right|$ is the absolute value of the Jacobian determinant, and log takes the logarithm of this value. The resulting scalar is also called the log-determinant. It measures the change in log-density when going from $h^{(i-1)}$ to $h^{(i)}$ under the transformation $f^{(i)}$.

Previous works [21, 25, 9, 11] suggest using a family of simple transformations in which the Jacobian $\partial h^{(i)}/\partial h^{(i-1)}$ is a triangular matrix, making the log-determinant simple to calculate.

$$log \left| det \left(\frac{\partial h^{(i)}}{\partial h^{(i-1)}} \right) \right| = sum \left(log \left| diag \left(\frac{\partial h^{(i)}}{\partial h^{(i-1)}} \right) \right| \right) \tag{9}$$

In equation 9, $sum()$ takes the sum over all vector elements, $log()$ takes the element-wise logarithm, and $diag()$ takes the diagonal of the Jacobian matrix.

4 SeismoFlow

In this section, we describe the proposed *SeismoFlow* model. *SeismoFlow* is a normalizing flow model, inspired by NICE [9], RealNVP [11], and Glow [3] models. Like in Glow, our model consists of a series of stacked flow blocks, which each block is composed of the following sequence:

ActoNorm Layer $\longrightarrow$ Invertible 1×1 Convolution $\longrightarrow$ Coupling Layer

Figure 1: Step Flow block.

In our model, we follow the design choice of [11], and at regular intervals, we factor out half of the dimensions. This approach is known as multi-scale architecture and is described in subsection 4.4.

Unlike previous works on this kind of model, we propose using of a multi-head self-attention layer [38] within the coupling layers that belong to the two last scale levels.

In the remainder of this section, we shortly explain each component that builds our model.

4.1 ActNorm layer

Introduced in [3], the Actnorm layer is proposed as an alternative to the standard batch normalization [39] for models trained with a small minibatch size. Similar to the batch normalization, the Actnorm layer normalizes the activations per channel. This normalization is done by an affine transformation that uses the scale and bias learnable parameters. The scale and bias parameters are initialized such that the activations after the Actnorm layer have per-channel zero mean and unit variance given an initial minibatch of data. Finally, the log-determinant is computed as follows:

$$log \left| det \left(\frac{\partial s \odot x + b}{\partial x} \right) \right| = h \cdot w \cdot sum(log|s|) \tag{10}$$

In equation 10, x is the layer input, s is the scale parameter, b is the bias parameter, $\odot$ is an element-wise product operation, h and w stand to the input height and width spatial dimensions.

4.2 Invertible 1×1 convolution

The Glow model [3] proposes to replace the usually used fixed permutations [9, 11] by a learned invertible 1×1 convolution. The weight matrix of this convolutions is initialized as a random rotation matrix, and they claim that since the number of channels in the layer's inputs and outputs is the same, the 1×1 convolution is a generalization of a permutation operator.

The invertible 1×1 convolution receives a tensor $x \in \mathbb{R}^{h \times w \times c}$ as input and applies the convolutional operator using its weight matrix $W \in \mathbb{R}^{c \times c}$ as a filter. Additionally, the weight matrix W is initialized to have an initial log-determinant of 0.

The log-determinant of this layer is computed as follows:

$$log \left| det \left(\frac{\partial conv2D(h; W)}{\partial h} \right) \right| = hight \cdot width \cdot log|det(W)| \tag{11}$$

4.3 Affine Coupling Layers

The affine coupling layer, introduced in [9, 11], is a simple bijective layer that is simple to invert and has a tractable Jacobian determinant. The input vector is split into two halves, and then complex dependencies are computed from one part and used to update the other part. In the end, the layer concatenates the split parts into a vector containing the same dimensions as the input. Given a D dimensional input x and $d < D$, the output y of an affine coupling layer follows the equation 12

$$\begin{cases} y_{1:d} = x_{1:d}; \\ y_{d+1:D} = x_{d+1:D} \odot exp(s(x_1:d)) + t(x_{1:d}) \end{cases} \tag{12}$$

where s and t stand for scale and translation and are functions from $\mathcal{R}^d \to R$, and $\odot$ is the element-wise product.

The Jacobian of this transformation is

$$J = \begin{bmatrix} \mathbb{I}_d & 0_{d \times (D-d)} \\ \frac{\partial y_{d+1:D}}{\partial x_{1:d}} & diag(exp(s(x_{1:d}))) \end{bmatrix} \tag{13}$$

4

where $diag(exp(s(x_{1:d})))$ is the diagonal matrix whose diagonal elements correspond to the vector $s(x_{1:d})$. A crucial observation is that this Jacobian is upper triangular, and therefore, we can efficiently compute its determinant as $exp\left[\sum_j s(x_{1:d})_j\right]$.

In the affine coupling layer, the operators s and t can be any arbitrarily complex functions, such as a neural network, because computing the Jacobian determinant of the layer does not involve calculating the Jacobian of those operators. For convenience, in the remaining of this paper, we call the operators s and t as $NN()$.

Finally, computing the inverse of the coupling layer is no more complicated than the forward propagation, and therefore, sampling is as efficient as inference for this layer. Equation 14 defines the inverse transformation of the affine coupling layer.

$$\begin{cases} x_{1:d} = y_{1:d}; \\ x_{d+1:D} = (y_{d+1:D} - t(y_{1:d})) \odot exp(-s(y_{1:d})) \end{cases} \tag{14}$$

Zero initialization

Following [3], we initialize the last $NN()$ layer with zeros. Thus, using this initialization, each affine coupling layer initially performs an identity function.

Split and concatenation

The affine coupling layer splits the input tensor h into two halves, and at the end, the layer undoes the split by concatenating the two halves into a single tensor again. Although other works suggest different types of splits, such as splitting using a checkerboard pattern along the spatial dimensions [11, 36], in this work, we follow the strategy proposed by [9] and [3], and only perform splits along the channel dimension.

4.4 Multi-scale architecture

Such as described in RealNVP [11], we implement a multi-scale architecture using a squeezing operation. The squeezing operation divides the image into patches of shape $2 \times 2 \times c$, then reshapes them into patches of shape $1 \times 1 \times 4c$, transforming an $s \times s \times c$ tensor into an $\frac{s}{2} \times \frac{s}{2} \times 4c$ tensor.

Our model is composed of a sequence of blocks, which at regular intervals, a squeeze operation is performed, defining L scale levels. At the beginning of each scale level, we perform a squeeze operation, and in the end, we factor out half of the dimensions.

Thus, at each scale, the spatial resolution is reduced and the number of hidden layer features is doubled. Additionally, all factored out variables are standardized to have zero mean and standard deviation one. The factored out variables correspond to intermediary representation levels that are fine-grained local features [18, 40, 11].

This approach reduces significantly the amount of computation and memory used by the model and distributes the loss function throughout the network. It is similar to guiding intermediate layers using intermediate classifiers [41].

5 Experimental Setup and Results

In this section, we present our experimental results, a short description of the dataset, the experimental setup, and the model hyper-parameters.

We start with the dataset description in sub-section 5.1; secondly, present the model architecture and hyper-parameters for both the *SeismoFlow* and the *Miniception* models in sub-section 5.2; then, we analyze the effects of varying the size of the augmentation on the classification performance in 5.3; finally, we close this section reporting the results for the seismogram quality classification task measured in a cross-validation setting in sub-section 5.4.

5.1 Dataset

We conducted extensive experiments on highly diverse seismic data, and present our results on that dataset. Our dataset comes from an offshore towed in a targeted region with 7993 shot-gathers from 8 cables each, thus containing a total of 63994 shot-gather images. In a shot-gather image, each column corresponds to a seismic trace recorded during the same seismic shot. Out of the total generated images, 5.223 were randomly chosen and manually classified by a geophysicist with *good*, *medium*, and *bad* labels according to a visual inspection of artifacts related to swell-noise and anomalous recorded amplitude. The resulting dataset is composed of 5.223 seismograms that are distributed between the *good*,

medium, and *bad* classes and with their respective frequencies of 66.68%, 31.54%, and 1.76%. Figure 5.1 shows one example per class of images.
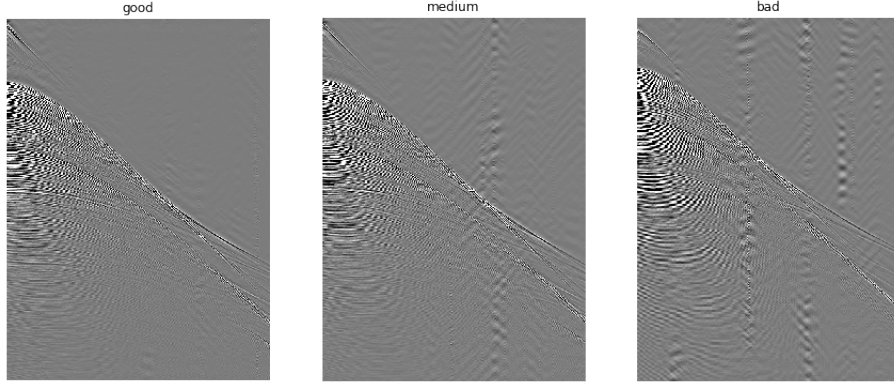

Figure 2: Per class seismogram example. In the left a sample from the good class. In the middle a sample from the medium class. In the left a sample from the bad class.

All images in our dataset have height resolution of 876, and the width varying between $[632, 639]$. Figure 5.1 shows the resolution distribution between dataset images.
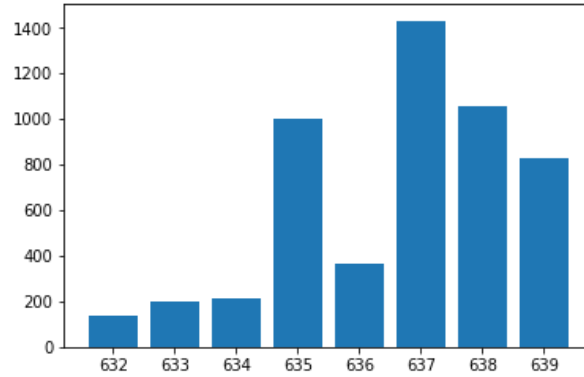

Figure 3: Distribution of images width sizes.

As it is explained in section 4, our model gradually reduces the image resolution by two several times. Due to that architectural choice, in our experiments we fix the size of all images to a fixed resolution of 640×896.

In the following sections we explain our experimental setup and dataset splits for each of our experiments. Additionally, we present the obtained results and analysis.

5.2 Experimental Setup

Our models share the same settings and hyper-parameters across all experiments. In the following, we present the settings for our models.

Generative Model

We use multi-scale architecture with 6 scale levels and 15 step-flow blocks per level. In the first four scale levels, we let each coupling layer *NN()* have three convolutional layers where the two hidden layers have ReLU activation functions and 96 channels. The first and last convolutions are 3×3, while the center convolution is 1×1. Additionally, before the last convolution, we apply a layer normalization [42].

6

In its turn, in the last scale level, we let each coupling layer *NN()* have one 4-headed self-attention layer [38], one layer normalization, 3×3 convolution layer with ReLu activation, and one 3×3 convolutional layers with its weights initialized with zeros, all with 96 filters.

Our model is trained using Adam Optimizer [43], with the default hyper-parameters, during 400 epochs. Due to memory constraints, we use a batch size of 1 image per iteration step. Additionally, the learning rate is scheduled to decay in a polynomial shape with a warm-up phase of 456 steps and a maximum learning rate of 0.0001.

Classification Model

We reuse all settings for the Miniception model [44], including hidden sizes and initialization.

The model is trained using Adam Optimizer [43], with the default hyper-parameters for 40 epochs.

5.3 Augmentations Effects

We begin our experiments by analyzing the effects of our generated samples on the *Miniception* model performance on the task of classifying the signal quality of seismograms. For this experiment, we performed the usual division of training, validation, and testing on our dataset using 70%, 10%, and 20% of the data for each respective partition. The partitions are stratified to maintain the original dataset distribution of classes. Additionally, the model is trained Adam Optimizer [43], with the default hyper-parameters and early stop with five epochs of patience for at maximum 100 epochs.

We present the performance curve of the F_1 metric, across ten runs of the learning process, using different augmentations sizes for low-frequency class. Figure 5.3 show the evolution of the F_1 score when varying the number of augmentations. The evaluation starts with zero augmentations and ends with 1000 augmentations for the minority class.
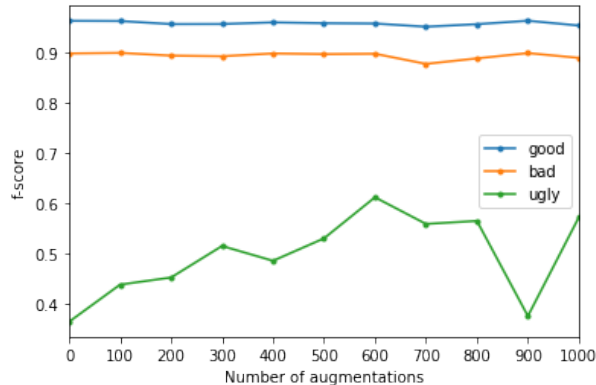

Figure 4: F_1 score curve when varying the augmentation size.

Since the F_1 score captures the balance between the $Precision$ and $Recall$, tending to the lowest value, accessing the figure above, we can conclude that for this set of partitions, 600 is the number of augmentations that achieves the most significant balanced gain in the metrics for all classes.

We believe that performing this search with cross-validation would give us a more robust result, but the execution time and computational power required for such an experiment prevents us from performing it. Thus, we use this result as a hint to the model's expected behavior to define the hyper-parameters of the next experiment that is presented in the following subsection.

5.4 Cross-Validation

In this section, we evaluate the quality of our methodology by augmenting the training set of our dataset using the samples generated by our generative model. We evaluate the $Precision$, $Recall$, and F_1 metrics, and its deviations, in a stratified 10-fold cross-validation setting [6]. In this setting, we split our data in 10 non-overlapping folds that are per-class stratified, fitting the *Miniception* model in 9 folds and leaving one out to test. In all cross-validation iterations, the *Miniception* model is trained for 40 epochs using the setup explained in section 5.2.

In Table 1, we present the obtained results, with and without augmenting the training set with our generated samples. For the augmented version, we generate 600 samples using the *SeismoFlow* model for each cross-validation iteration. Additionally, to avoid passing any information from the test folds to the training folds, the augmentations are generated by only using data from the training set of each cross-validation iteration.

Table 1: Cross-Validation per-class average precision, recall, and F_1 metrics.

Class	Not Augmented			Augmented		
	$Precision$ (%)	$Recall$ (%)	F_1 (%)	$Precision$ (%)	$Recall$ (%)	F_1 (%)
Good	95.1 ± 0.57	$\mathbf{97.1 \pm 0.73}$	96.0 ± 0.25	$\mathbf{95.4 \pm 0.47}$	97.4 ± 0.32	$\mathbf{96.4 \pm 0.21}$
Medium	90.9 ± 1.23	88.6 ± 1.46	89.6 ± 0.55	$\mathbf{92.8 \pm 0.54}$	$\mathbf{88.7 \pm 1.17}$	$\mathbf{90.6 \pm 0.59}$
Bad	65.3 ± 4.51	42.5 ± 4.69	49.0 ± 3.82	$\mathbf{68.3 \pm 4.34}$	$\mathbf{70.4 \pm 2.47}$	$\mathbf{68.5 \pm 2.84}$

As can be seen from the table, our augmentations yield consistent improvements in metrics, not only for the bad class but also for the other classes. We can note that when adding the augmentations, the model improves 8.62% in the precision, 48.5% in the recall, and 38.2% in the F_1 scores of the low-frequency class. Furthermore, we can observe these improvements as long as the values for these metrics on the other classes are not impaired and thus, improving the model's overall accuracy.

Table 2 show averaged metrics for both versions of the model, with and without data augmentation. We can note that, when augmenting the training data, the model gets a 13.9% improvement on the averaged F_1 metric.

Table 2: Cross-Validation average precision, recall, and F_1 metrics.

Model	$Precision$ (%)	$Recall$ (%)	F_1 (%)
Augmented	$\mathbf{94.4 \pm .003}$	$\mathbf{94.3 \pm .003}$	$\mathbf{94.2 \pm 00.3}$
Not Augmented	$93.6 \pm .002$	$93.7 \pm .002$	$93.5 \pm .002$

6 Conclusion

A common problem in machine learning classification tasks is the imbalanced class problem [1]. The class imbalance problem is a challenge in machine learning classification tasks. The problem occurs when there is a rare and very low-frequency class in the training set, making many machine learning algorithms, such as neural networks, struggle to learn to classify the low-frequency class correctly [2].

In this work, we propose a flow-based generative model to create synthetic samples, aiming to address the class imbalance. Inspired by the Glow model [3], it uses interpolation on the learned latent space to produce synthetic samples for the smallest class. We apply our approach to the development of a seismogram signal quality classifier.

We introduce a dataset composed of 5.223 seismograms that are distributed between the *good*, *medium*, and *bad* classes and with their respective frequencies of 66.68%, 31.54%, and 1.76%.

We evaluate our methodology on a stratified 10-fold cross-validation setting [6], using the *Miniception* model [] as a baseline and assessing the effects of adding the generated samples on the training set of each iteration.

To avoid transferring from the test fold set to the training folds set, when augmenting the minority class, we compute the augmentations, only using the data designed to the training set of each cross-validation iteration. In our experiments, we analyze the effects of adding the generated seismograms by comparing the *precision*, *recall*, and F_1 metrics of each class. When augmenting the training set with our generated samples, we achieve an improvement of 13.9% on the F_1 score of the low-frequency class, while not hurting the metric value for the other classes and thus observing an improvement on the overall accuracy. Finally, our empirical findings indicate that our method can generate high-quality synthetic samples with realistic looking and sufficient plurality to help a second model to overcome the class imbalance problem. We believe that our results are a step forward in solving both the task of seismogram signal quality classification and class imbalance.

Acknowledgment

References

[1] Xu-Ying Liu, Jianxin Wu, and Zhi-Hua Zhou. Exploratory undersampling for class-imbalance learning. *IEEE Transactions on Systems, Man, and Cybernetics, Part B (Cybernetics)*, 39:539–550, 2009.

[2] Salman Hameed Khan, Munawar Hayat, Mohammed Bennamoun, Ferdous Ahmed Sohel, and Roberto Togneri. Cost-sensitive learning of deep feature representations from imbalanced data. *IEEE Transactions on Neural Networks and Learning Systems*, 29:3573–3587, 2015.

[3] Diederik P. Kingma and Prafulla Dhariwal. Glow: Generative flow with invertible 1x1 convolutions. In *NeurIPS*, 2018.

[4] Daniel Chevitarese, Daniela Szwarcman, Reinaldo Mozart D Silva, and Emilio Vital Brazil. Transfer learning applied to seismic images classification. *AAPG Annual and Exhibition*, 2018.

[5] Andrew Valentine and John H. Woodhouse. Approaches to automated data selection for global seismic tomography. 2010.

[6] Ron Kohavi. A study of cross-validation and bootstrap for accuracy estimation and model selection. In *Proceedings of the 14th International Joint Conference on Artificial Intelligence - Volume 2*, IJCAI'95, pages 1137–1143, San Francisco, CA, USA, 1995. Morgan Kaufmann Publishers Inc.

[7] Diederik P. Kingma and Max Welling. Auto-encoding variational bayes. *CoRR*, abs/1312.6114, 2013.

[8] Alex Graves. Generating sequences with recurrent neural networks. *ArXiv*, abs/1308.0850, 2013.

[9] Laurent Dinh, David Krueger, and Yoshua Bengio. Nice: Non-linear independent components estimation. *CoRR*, abs/1410.8516, 2014.

[10] Aäron van den Oord, Nal Kalchbrenner, and Koray Kavukcuoglu. Pixel recurrent neural networks. In *ICML*, 2016.

[11] Laurent Dinh, Jascha Sohl-Dickstein, and Samy Bengio. Density estimation using real nvp. *ArXiv*, abs/1605.08803, 2016.

[12] Ian J. Goodfellow, Jean Pouget-Abadie, Mehdi Mirza, Bing Xu, David Warde-Farley, Sherjil Ozair, Aaron C. Courville, and Yoshua Bengio. Generative adversarial networks. *ArXiv*, abs/1406.2661, 2014.

[13] Sepp Hochreiter and Jürgen Schmidhuber. Long short-term memory. *Neural Computation*, 9:1735–1780, 1997.

[14] Aaron van den Oord, Nal Kalchbrenner, Oriol Vinyals, Lasse Espeholt, Alex Graves, and Koray Kavukcuoglu. Conditional image generation with pixelcnn decoders. In *NIPS*, 2016.

[15] Aäron van den Oord, Sander Dieleman, Heiga Zen, Karen Simonyan, Oriol Vinyals, Alex Graves, Nal Kalch-brenner, Andrew W. Senior, and Koray Kavukcuoglu. Wavenet: A generative model for raw audio. In *SSW*, 2016.

[16] Tero Karras, Timo Aila, Samuli Laine, and Jaakko Lehtinen. Progressive growing of gans for improved quality, stability, and variation. *ArXiv*, abs/1710.10196, 2017.

[17] Aditya Grover, Manik Dhar, and Stefano Ermon. Flow-gan: Combining maximum likelihood and adversarial learning in generative models. In *AAAI*, 2017.

[18] Danilo Jimenez Rezende, Shakir Mohamed, and Daan Wierstra. Stochastic backpropagation and approximate inference in deep generative models. In *ICML*, 2014.

[19] Ronald J. Williams. Simple statistical gradient-following algorithms for connectionist reinforcement learning. *Machine Learning*, 8:229–256, 1992.

[20] Lars Maaløe, Casper Kaae Sønderby, Søren Kaae Sønderby, and Ole Winther. Auxiliary deep generative models. *ArXiv*, abs/1602.05473, 2016.

[21] Danilo Jimenez Rezende and Shakir Mohamed. Variational inference with normalizing flows. *ArXiv*, abs/1505.05770, 2015.

[22] Tim Salimans, Diederik P. Kingma, and Max Welling. Markov chain monte carlo and variational inference: Bridging the gap. In *ICML*, 2014.

[23] Mark N. Gibbs and David J. C. MacKay. Variational gaussian process classifiers. *IEEE transactions on neural networks*, 11 6:1458–64, 2000.

[24] Yuri Burda, Roger B. Grosse, and Ruslan Salakhutdinov. Importance weighted autoencoders. *CoRR*, abs/1509.00519, 2015.

[25] Diederik P. Kingma, Tim Salimans, Rafal Józefowicz, Xi Chen, Ilya Sutskever, and Max Welling. Improving variational autoencoders with inverse autoregressive flow. In *NIPS*, 2016.

[26] Brendan J. Frey. Graphical models for machine learning and digital communication. 1998.

[27] Hugo Larochelle and Iain Murray. The neural autoregressive distribution estimator. In *AISTATS*, 2011.

[28] Mathieu Germain, Karol Gregor, Iain Murray, and Hugo Larochelle. Made: Masked autoencoder for distribution estimation. In *ICML*, 2015.

[29] Kaiming He, Xiangyu Zhang, Shaoqing Ren, and Jian Sun. Deep residual learning for image recognition supplementary materials. 2016.

[30] Kaiming He, Xiangyu Zhang, Shaoqing Ren, and Jian Sun. Identity mappings in deep residual networks. *ArXiv*, abs/1603.05027, 2016.

[31] Lucas Theis and Matthias Bethge. Generative image modeling using spatial lstms. In *Proceedings of the 28th International Conference on Neural Information Processing Systems - Volume 2*, NIPS'15, pages 1927–1935, Cambridge, MA, USA, 2015. MIT Press.

[32] Rafal Józefowicz, Oriol Vinyals, Mike Schuster, Noam Shazeer, and Yonghui Wu. Exploring the limits of language modeling. *ArXiv*, abs/1602.02410, 2016.

[33] Oriol Vinyals, Samy Bengio, and Manjunath Kudlur. Order matters: Sequence to sequence for sets. *CoRR*, abs/1511.06391, 2015.

[34] Aäron van den Oord, Yazhe Li, Igor Babuschkin, Karen Simonyan, Oriol Vinyals, Koray Kavukcuoglu, George van den Driessche, Edward Lockhart, Luis C. Cobo, Florian Stimberg, Norman Casagrande, Dominik Grewe, Seb Noury, Sander Dieleman, Erich Elsen, Nal Kalchbrenner, Heiga Zen, Alex Graves, Helen King, Tom Walters, Dan Belov, and Demis Hassabis. Parallel wavenet: Fast high-fidelity speech synthesis. *ArXiv*, abs/1711.10433, 2017.

[35] Christos Louizos and Max Welling. Multiplicative normalizing flows for variational bayesian neural networks. In *ICML*, 2017.

[36] Jonathan Ho, Xi Chen, Aravind Srinivas, Yan Duan, and Pieter Abbeel. Flow++: Improving flow-based generative models with variational dequantization and architecture design. In *ICML*, 2019.

[37] Aidan N. Gomez, Mengye Ren, Raquel Urtasun, and Roger B. Grosse. The reversible residual network: Back-propagation without storing activations. *ArXiv*, abs/1707.04585, 2017.

[38] Ashish Vaswani, Noam Shazeer, Niki Parmar, Jakob Uszkoreit, Llion Jones, Aidan N. Gomez, Lukasz Kaiser, and Illia Polosukhin. Attention is all you need. In *NIPS*, 2017.

[39] Sergey Ioffe and Christian Szegedy. Batch normalization: Accelerating deep network training by reducing internal covariate shift. *ArXiv*, abs/1502.03167, 2015.

[40] Ruslan Salakhutdinov and Geoffrey E. Hinton. Deep boltzmann machines. In *AISTATS*, 2009.

[41] Chen-Yu Lee, Saining Xie, Patrick W. Gallagher, Zhengyou Zhang, and Zhuowen Tu. Deeply-supervised nets. *ArXiv*, abs/1409.5185, 2014.

[42] Jimmy Ba, Jamie Ryan Kiros, and Geoffrey E. Hinton. Layer normalization. *ArXiv*, abs/1607.06450, 2016.

[43] Diederik P. Kingma and Jimmy Ba. Adam: A method for stochastic optimization. *CoRR*, abs/1412.6980, 2014.

[44] Eduardo Betine Bucker, Antonio José Grandson Busson, Ruy Luiz Milidiú, Sérgio Colcher, Bruno Pereira Dias, and André Bulcão. A deep convolutional network for seismic shot-gather image quality classification, 2019.